NANO EXPRESS

PAPER

Zinc oxide tetrapods as novel field emitters with low turn-on voltage

Filippo Giubileo[1], Enver Faella[2], Arun Kumar[3,4], Sebastiano De Stefano[3], Loredana Viscardi[3], Kimberly Intonti[3], Ofelia Durante[3], Aniello Pelella[5], Adolfo Mazzotti[5], Nadia Martucciello[1], Eugeniy Beliayev[6,7], Yogendra Kumar Mishra[6], Maurizio Passacantando[2] and Antonio Di Bartolomeo[3]

[1] CNR-SPIN Salerno, via Giovanni Paolo II n.132, 84084 Fisciano, Italy
[2] Department of Physical and Chemical Science, University of L'Aquila, Via Vetoio, Coppito, 67100, L'Aquila, Italy
[3] Department of Physics 'E.R. Caianiello', University of Salerno, via Giovanni Paolo II n.132, 84084, Fisciano, Italy
[4] Department of Science and Engineering of the Environment and Urban Planning, Polytechnic University of Marche, Via Brecce Bianche 12, 60131, Ancona, Italy
[5] Dipartimento di Fisica, Università degli studi di Roma Tor Vergata, via della Ricerca Scientifica 1, 00133, Rome, Italy
[6] Smart Materials, Mads Clausen Institute, University of Southern Denmark, Alsion 2, DK-6400, Sønderborg, Denmark
[7] B. Verkin Institute for Low Temperature Physics and Engineering, 47 Nauky Avenue, Kharkiv, 61103, Ukraine

E-mail: filippo.giubileo@spin.cnr.it **and** adibartolomeo@unisa.it

Keywords: field emission, zinc oxide, tetrapods, turn-on voltage, fowler-nordheim model

OPEN ACCESS

RECEIVED
6 November 2024

REVISED
2 December 2024

ACCEPTED FOR PUBLICATION
10 December 2024

PUBLISHED
18 December 2024

Abstract

We investigate the field emission properties of tetrapod-shaped zinc oxide (ZnO) micro and nanostructures prepared using a flame transport synthesis approach. Using a piezo-driven metallic tip as an anode, we performed a local characterization from the apex of a tetrapod arm, where the effective emitting area was limited below 1 μm^2. This configuration allows extremely low turn-on voltages, of 7 V, and a field enhancement factor of 70 at an anode-cathode distance of 600 nm. The experimental data were analyzed using the Fowler–Nordheim model, evidencing a non-monotonous dependence of the turn-on field and the field enhancement factor on the cathode-anode separation distance in the range of 100–900 nm. The ZnO tetrapods demonstrated good current stability, highlighting their potential for high-performance, low-consumption electron-emitting devices with very low turn-on voltage.

Introduction

Zinc Oxide (ZnO) is an *n*-type semiconductor (II-VI group material) characterized by a wide and direct bandgap of 3.37 eV and an exciton-binding energy of about 60 meV at room temperature. ZnO is an abundant, cost-effective, chemically stable, non-toxic material with an inherent hexagonal wurtzite crystal structure (non-centrosymmetric system with a large saturation velocity of about 3.2×10^7 cm s^{-1}), high electron mobility, and good biocompatibility [1]. The hexagonal wurtzite crystal structure enables ZnO oxide to be grown with almost any imaginary one-dimensional morphology and a large variety of micro and nanostructures, such as nanoplatelets [2], nanobelts [3], nanoflowers [4], nanowires [5], and nanorods [6], etc from ZnO have been synthesized, characterized, and utilized for applications [7]. Among the various nanostructures, the tetrapod shaped ZnO micro and nanostructures have garnered significant attention due to their unique three-dimensional (3D) spatial structure [7], superior optical properties [8], and relatively lower density of native defects compared to other morphologies [9]. A ZnO tetrapod is an inherent structure built out of four interconnected 1D ZnO rods interconnected via a central crystalline ZnO core at an angle of around 105 to 110 degrees with respect to each other in a symmetrical manner. The complex 3D configuration of ZnO tetrapods allows the creation of robust interconnected 3D networks with desirable high porosities and mechanical strengths. These tetrapods form a self-assembled 3D hierarchical architecture irrespective of how they are placed together, and further heating at high temperatures allows the formation of strong interconnections among the arms, providing mechanical stability to the network [7, 10]. The ZnO tetrapods are widely used as reinforcing agents in composite materials [11] and show great potential for applications in biomedical engineering [12, 13].

Moreover, ZnO nanostructures are also promising candidates for high-performance field emission (FE) devices owing to their low work function, high thermal and mechanical stability, and excellent oxidation resistance, even in harsh environments [14].

Field emission is a quantum phenomenon extremely relevant to the realization of cold sources of electrons unlike the thermionic sources in which thermal energy must be provided to electrons in the emitter in order to favor their emission [15]. In the FE process, the electrons near the Fermi level escape from a surface by tunnelling through the potential barrier at the emitter/vacuum interface. The process is favored by the application of a strong electric field that modifies the barrier, making it triangular, lower, and thinner. A nanostructured surface is a better emitter because it causes the enhancement of the local electric field, enabling the emission of measurable currents at a reduced field intensity of the order of a few V/μm.

Wide research activity has been reported in the last years concerning the field emission properties of various ZnO nanostructures [16–18]. Recent research on enhancing the FE properties of ZnO nanostructures has focused on two main strategies: optimizing the geometric factors by increasing alignment [19], and aspect ratio [20], or reducing the tip size of the nanostructures; and improving conductivity [21] and reducing the work function through selective element doping [22], material combination [23, 24], or ion implantation [25]. Almost in all cases, despite a relatively low turn-on field reported, the FE setups used in those experiments need a large bias applied to the anode in the order of KV to activate the FE phenomenon in ZnO tetrapods [26–30]. For instance, tetrapod-like ZnO nanostructures synthesized by rapid evaporation were investigated using a transparent anode imaging technique with a bias range up to 1 kV and an anode 0.1 mm away from the emitter. As a consequence, bias above 0.1 kV was necessary to activate the emission [30].

In this paper, we investigate the field emission properties of ZnO tetrapods synthesized by the flame transport synthesis (FTS) technique by applying a tip-shaped anode configuration. A piezo-driven metallic tip is exploited as an anode in close proximity to the emitter to get a local characterization of the FE properties, with electrons emitted from the apex of a single arm of a ZnO tetrapod. We demonstrate that FE current can be activated by a turn-on voltage as small as 7V. We also report a complete characterization of the emission parameters, such as turn-on voltage, turn-on field, and field enhancement factor, as a function of the cathode-anode separation distance.

Experimental methods

Tetrapod-shaped ZnO structures were synthesized using the flame transport synthesis (FTS) technique, and the procedure has been reported in previous work [31]. In this process, a ceramic crucible is filled with zinc microparticle (around 5 μm diameter) and polyvinyl butyral (PVB) powders in a weight ratio of 1:2 and is heated in a simple muffle oven at 900 °C for 30 min. The Zn particles are metallic precursors and sacrificial PVB's role is just to generate the flame. The Zn microparticles are converted in Zn atomic vapour in the flame and with the available native oxygen (controlled by flame) the growth of ZnO micro-nano tetrapods occurs by solid-vapour-solid growth mechanism. After 30 minutes, the furnace is allowed to naturally cool which leads to the formation of snow-like white powder out of ZnO tetrapods. These tetrapods were carefully harvested and utlized for field emission studies. X-ray diffraction (XRD) measurements on ZnO tetrapods have been performed using a Bruker D5000 diffractometer with excitation source Cu-Kα (wavelength, $\lambda = 1.54056$ Å) working in Bragg–Brentano geometry. Morphology and electrical characterization were carried out at room temperature and at a pressure of 10^{-6} mbar inside Scanning Electron Microscopy (SEM) model LEO 1530 (by Zeiss, Germany) equipped with piezo-electrically controlled metallic probes (MM3A-EM micromanipulator by Kleindiek Nanotechnik, Germany) having a step resolution of 5 nm. To realize the electrical measurements, the metallic probes were used as electrodes connected through high vacuum feedthrough to a semiconductor parameter analyzer Keithley 4200-SCS (by Tektronix, USA) working as a source-measurement unit with a current resolution better than 0.1 pA and with a voltage range source ± 200 V.

The field emission measurements were performed by positioning one probe electrode (anode) at a controlled distance from the emitting surface (cathode), applying to it a high positive bias to favor the extraction of electrons from the ZnO tetrapods, and by measuring the current flowing through the vacuum gap between the cathode and the anode. Thus, our setup allowed for *in situ* measurements of the emission current as a function of both the applied voltage (V) and the anode-cathode separation distance (d). Unlike the static configurations commonly reported in the literature, where the anode is fixed, and only the applied voltage is varied, our approach provides a more comprehensive understanding of how geometric factors influence emission properties. Using a movable anode is particularly advantageous for investigating the effect of anode-cathode distance on the emission onset field (E_{on}) and field enhancement factor (β). In fact, our setup allowed us to study the dynamic behavior of emission current under varying geometric conditions, identifying optimal conditions for field emission performance from a single ZnO tetrapod. This *in situ* methodology offers unique insights into

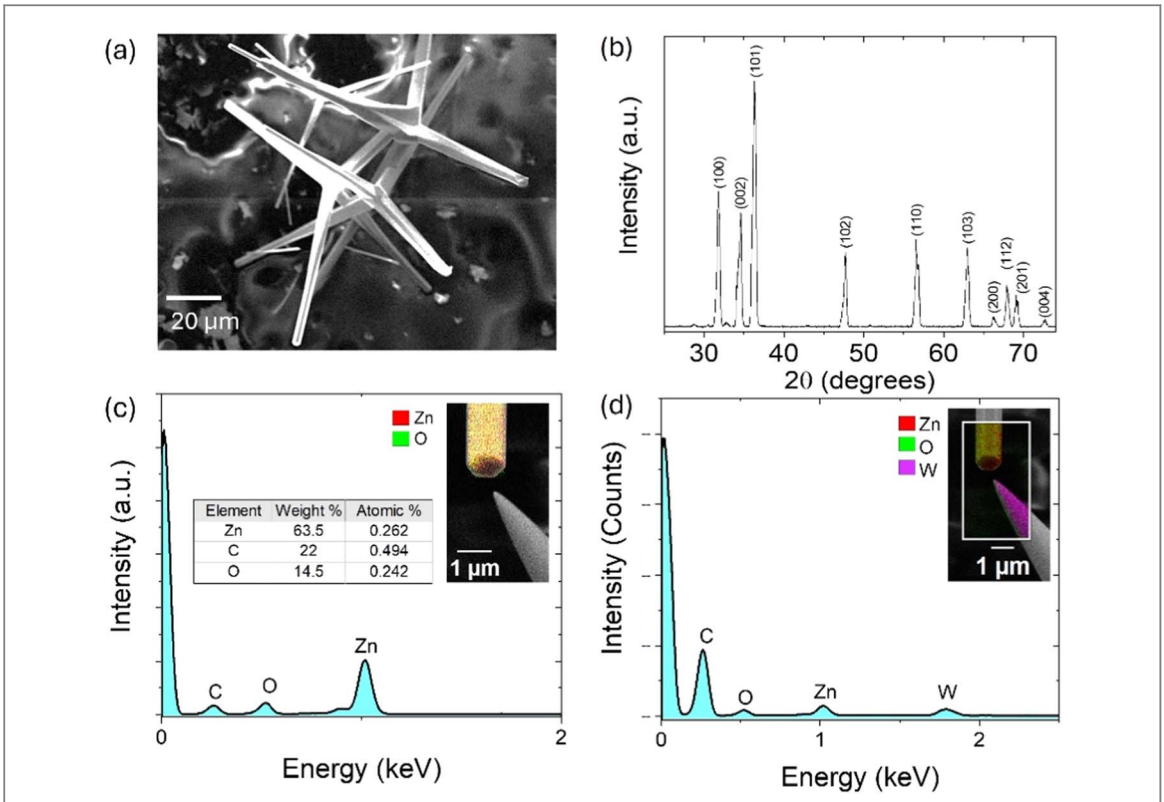

Figure 1. (a) SEM images of ZnO tetrapods, (b) XRD pattern measured for ZnO tetrapods, showing a typical wurtzite structure with all the peaks indexed in the standard hexagonal wurtzite cell (P63mc), (c) EDX spectra over the ZnO single arm, (d) EDX spectra over the ZnO single arm and W anode tip.

the field emission characteristics, bridging the gap between theoretical predictions and experimental observations.

Results and discussion

Figure 1(a) shows the SEM image of the ZnO tetrapods clustered over the silver paste. It can be seen that the tetrapods consist of four arms branching from the common centre and the angles between arms are almost equivalent. The length of arms is within the range of 20–30 μm. Figure 1(b) shows the XRD patterns measured for the ZnO tetrapods. The observed peaks can be easily assigned to the pure hexagonal phase of ZnO, space group P63mc, in agreement with the standard values (JCPDS card. no. 36-1451). The clear and sharp peaks indicated that the as-prepared tetrapods possess a high degree of crystallinity. At least no diffraction peaks indicating the presence of interstitial Zn or other structural impurities are detected in the spectrum, confirming the optimal morphology of our samples with high crystal quality.

Figure 1(c) shows the SEM energy-dispersive x-ray (EDX) spectra of the ZnO tetrapods, confirming the stoichiometric ratio of the elements; the inset shows the ZnO tetrapod portion where the EDX was recorded. Figure 1(d) and inset depict the EDX spectra confirming the tungsten (W) anode in a close approximation with the ZnO tetrapod.

Electrical measurements were performed in a high vacuum with the sample placed inside the SEM chamber at a pressure of 10^{-6} mbar. A schematic of the experimental setup is reported in figure 2(a). As the initial step, the W tip (anode) is placed in contact with the Zn tetrapods to realize a direct electrical contact (see figure 2(b)), while the cathode is connected to the back side by silver paint to realize an ohmic contact. The current–voltage (I-V) characteristic measured in such contact configuration is reported in figure 2(c). The curve is linear evidencing an ohmic behavior with a resistance of about 140 kΩ. If the tip is retracted at a large distance from the ZnO tetrapod (> 2 μm), no current can be measured in the circuit, as demonstrated by the I-V characteristic reported in figure 2(d). The curve represents the setup floor noise, with a level of 10^{-14} A.

Taking advantage of the piezo-driven nanomanipulator, we carefully positioned the W-tip anode at short distances from the ZnO tetrapod arm, in a range below 1 μm. In this configuration, by applying a strong electric field, i.e., a high positive bias to the W tip, we can favor the emission of electrons from the ZnO because the potential barrier becomes thinner and triangular, and electrons can escape by tunnelling through the ZnO/

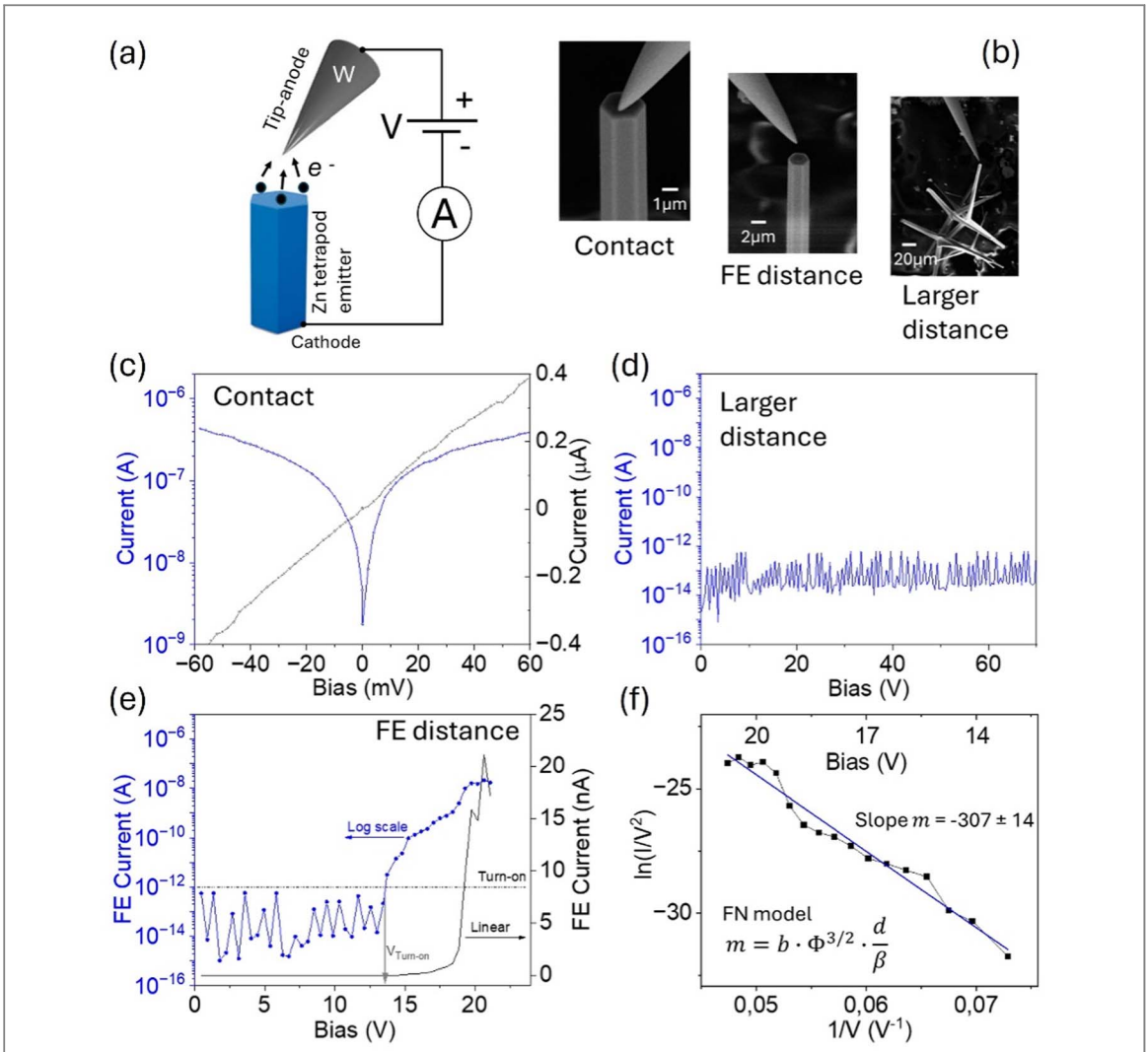

Figure 2. (a) Schematic of the FE setup in which a tungsten tip is exploited as an anode to collect electrons from the emitter (ZnO tetrapod). (b) SEM images of different configurations with the tip in 'contact' with the cathode at a small '(FE) distance' from the surface and at a large distance (larger than 2 μm). (c) Current–voltage (I-V) curve, reported in log (left) and linear (right) scale, measured when the tip is in contact with the tetrapod, showing a resistive behavior. (d) I-V measured with the tip at a distance greater than 2μm from the ZnO tetrapod: no electrons can travel through the gap, and the setup floor noise is measured. (e) I-V measured with the tip positioned at distance d = 200 nm. (f) Fowler–Nordheim plot and its linear fit.

vacuum potential barrier. In figure 2(e), we show the I-V characteristic measured with the tip anode positioned at a distance d = 200 nm from the tetrapod surface. We notice that by raising the positive bias, the current is not flowing through the device for low bias till reaching a sufficiently intense value to switch on the emission (here, we define the turn-on voltage, V_{ON}, as the voltage necessary to cause a current of 1 pA). After the turn-on V_{ON}= 13.5 V, the FE current rapidly increases for increasing voltage, showing a current increase of more than four orders of magnitude caused by a voltage increase of less than 10 V.

To confirm that the measured current is due to the FE phenomenon, we analyze the experimental data within the standard Fowler–Nordheim (FN) model [32]. It provides a simple formula for the FE current:

$$I = S\frac{aE_{local}^2}{\varphi}\exp\left(-b\frac{\varphi^{3/2}}{E_{local}}\right) \quad (1)$$

In which S is the emitting area, $a = 1.54 \times 10^{-6}$ A eV V^{-2} and $b = 6.83 \times 10^9$ V m^{-1} eV$^{-3/2}$ are constants, E_{local} is the local electric field on the emitter surface, φ is the ZnO workfunction. The local electric field is caused by the applied bias V to the tip anode (the cathode being grounded) according to the formula $E_{local} = \beta V d^{-1}$ where d is the cathode-anode separation distance and β is the field enhancement factor that takes into account the local amplification of the field due to the emitter geometry.

The standard procedure to confirm the FE nature of the measured current is to verify the linearity of the so-called FN-plot, i.e. $ln(I/V^2)$ versus $1/V$. This is widely considered a valid approach to obtain a first-approximation demonstration of the field emission from the various nanostructures [33]. So, we will apply this powerful method despite being aware that it has been developed for a simplified model with a flat metallic

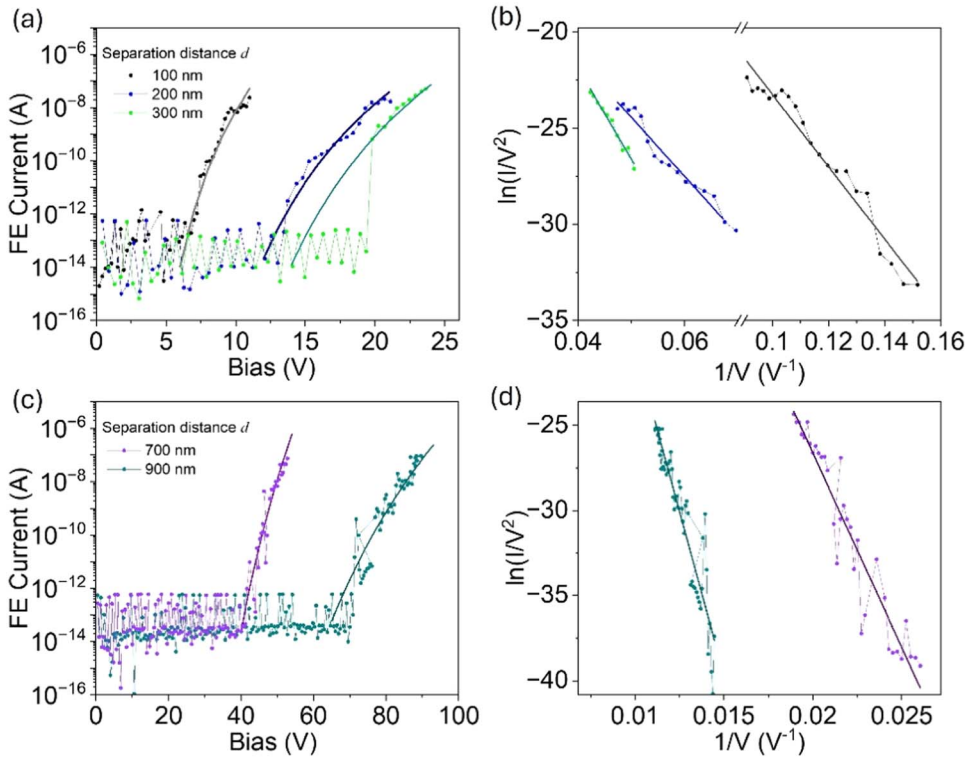

Figure 3. Current–Voltage curves measured in the FE regime for different cathode-anode separation distances. (a) I-V curves are measured for very small distances (100–300 nm); (b) FN plots and corresponding linear fits, showing the FE nature of the curves in (a); (c) I-V curves measured for larger distances (up to 900 nm); (d) FN plots and corresponding linear fits, showing FE nature of the curves in (c).

surface, a triangular potential barrier, and zero kelvin temperature. For the sake of completeness, we mention here that several studies [34] have extended the FN model to take into account the dimensionality of the emitters [35], small and large curvatures [36], areas with non-homogeneous workfunction [37], finite temperature [38], etc.

Following this approach, we show in figure 2(f) the FN plot for the I-V curve reported in figure 2(e). The experimental data are compared to their linear fit, which clearly confirms the FE nature of the measured current. Moreover, considering that the slope m of the FN plot can be expressed as $m = -(bd\varphi^{3/2})/\beta$, we can use the linear fit, and the slope, to estimate the field enhancement factor β. In particular, being $m = 307 \pm 14$ the slope extracted by the linear fit, we can easily calculate $\beta \approx 50$ for an anode-cathode separation distance of 200 nm.

The piezo-driven nanomanipulator, on which the W tip (anode) is mounted, gave us the possibility to vary the cathode-anode separation distance and perform a characterization of the FE properties as a function of d. We first performed the measurements in a range from 100 nm up to 300 nm, i.e. with a tip very close to the emitting surface. The I-V curves measured for different d values are presented in figure 3(a). As expected, we see that by increasing the separation distance, it is necessary to apply a larger bias in order to extract electrons from the emitter, i.e., a larger separation causes a larger turn-on voltage. The corresponding linear FN plots are reported in figure 3(b), and they confirm the FE nature of the measured current. We point out that we limited our working (I, V) range in order to keep the FE current below 1μA to avoid the current density being too high that could burn/destroy the emitter. We consider that according to simulation models existing in literature, when the tip anode is at 200 nm from the emitter surface, the effective emitting area is limited to about 0.1 μm^2, that means to reach a current density as high as 10^7 A m^{-2}. We also performed the FE characterization in a larger separation range (up to 900 nm). I-V characteristics measured at 700 nm and 900 nm are reported in figure 3(c), and the corresponding FN plots in figure 3(d). As further confirmation of the correctness and applicability of the FN model, we also compared the experimental data (dotted curves in figures 3(a) and (c)) of the I-V characteristics with the theoretical expectation (solid lines) calculated according to equation (1).

In figure 4(a), we summarize the turn-on voltage data as a function of the cathode-anode separation distance, evidencing that V_{ON} increases for increasing d. We notice that the rapidity of the increase is different, allowing us to identify two different regimes: a regime in which the V_{ON} increases slowly with d for separation distances below 500 nm and a regime with a faster increase for 500 nm $< d <$ 900 nm. The minimum recorded turn-on voltage V_{ON} of about 7V was obtained when the W tip was approached to the minimum distance of

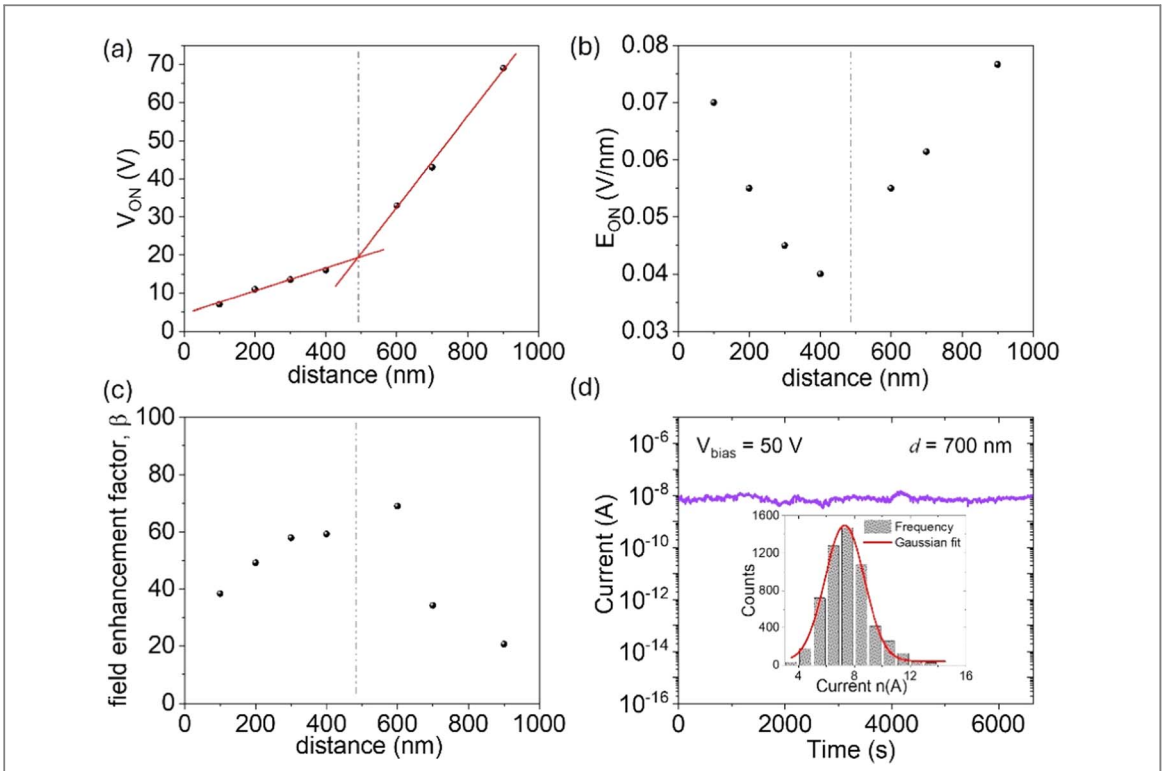

Figure 4. (a) Turn-on voltage as a function of the cathode-anode separation distance d. Two different regions can be identified by two different slopes. (b) Turn-on field as a function of d. (c) Dependence of the field enhancement factor on d. (d) FE current stability was measured at the fixed bias of 50 V, keeping the anode tip at a fixed distance of 700 nm.

100 nm. We also estimated the corresponding turn-on field E_{ON}. Interestingly, we notice that the dependence of E_{ON} versus d (see figure 4(b)) is non-monotonous, with a minimum in correspondence to the change of regime. The minimum E_{ON} is about 0.04 V nm^{-1} at $d = 400$ nm.

For each FN plot, we can use the slope of the linear fit to extract the field enhancement factor β as a function of d. The plot, reported in figure 4(c), evidences that β increases for increasing d when moving in the small distance range. Vice versa, for $d > 500$ nm, i.e. in the region of larger distances, we found that β is a decreasing function of d. The maximum reported value is $\beta = 70$ for $d = 600$ nm. The non-monotonous behavior of the field enhancement factor has already been observed when characterizing other nanostructures in separation ranges of similar dimensions, as for few-layer MoS_2 [39] and for InSb nanopillars [40].

A further crucial parameter, together with the turn-on field and the field enhancement factor, to characterize the FE properties of a nanostructure, is the time stability of the emitted current [41]. To demonstrate this capability of the ZnO tetrapod, we positioned the anode tip at a fixed distance from the emitter ($d = 700$ nm) and applied a fixed bias of 50 V on the tip anode. The FE current versus time is reported in figure 4(d), showing a stable current for several minutes. No current degradation has been observed during the test. From a statistical point of view, we can analyze the current fluctuations: the inset of figure 4(d) evidences that current values have a Gaussian distribution around an average value of about 7.5 nA with a standard variation of 1.5 nA.

Conclusions

In conclusion, ZnO tetrapods synthesized via flame transport synthesis have demonstrated excellent field emission properties, characterized by a low turn-on voltage of 7 V and a high field enhancement factor of up to 70. The experimental results, analyzed using the Fowler–Nordheim model, revealed a non-monotonous dependence of the turn-on field and field enhancement factor on the cathode-anode separation distance, indicating distinct emission regimes. Additionally, the ZnO tetrapods exhibited stable electron emission over time, confirming their potential for use in high-performance electron-emitting devices requiring low operating voltages. These findings highlight the promise of ZnO tetrapods for future applications in advanced low-consumption field emission technologies.

Acknowledgments

YKM acknowledges to Danish Agency for Higher Education and Science (UFM) for NANOCHEM (national infrastructure UFM 5229-00010B), Denmark, BHJ Fonden, and Fabrikant Mads Clausen Fonden for support. YKM also appreciates the financial support from Carlsberg Foundation Denmark for the SARU (Scholars at Risk from Ukrainian Universities) Fellowship to Dr Eugene Beliayev to work at SDU Sønderborg (in a critical war situation).

Conflicts of interest

The authors declare no conflict of interest.

Data availability statement

No repository available due to high cost. The data that support the findings of this study are available upon reasonable request from the authors.

ORCID iDs

Filippo Giubileo https://orcid.org/0000-0003-2233-3810
Enver Faella https://orcid.org/0000-0002-5782-6685
Arun Kumar https://orcid.org/0000-0002-6333-2198
Sebastiano De Stefano https://orcid.org/0009-0007-8492-0857
Loredana Viscardi https://orcid.org/0000-0002-9674-7752
Kimberly Intonti https://orcid.org/0000-0003-1755-183X
Ofelia Durante https://orcid.org/0000-0002-3539-3858
Aniello Pelella https://orcid.org/0000-0002-3831-0210
Adolfo Mazzotti https://orcid.org/0009-0008-9021-7874
Nadia Martucciello https://orcid.org/0000-0003-1019-1587
Eugeniy Beliayev https://orcid.org/0000-0001-6991-1345
Yogendra Kumar Mishra https://orcid.org/0000-0002-8786-9379
Maurizio Passacantando https://orcid.org/0000-0002-3680-5295
Antonio Di Bartolomeo https://orcid.org/0000-0002-3629-726X

References

[1] Gulab H *et al* 2024 Advancements in zinc oxide nanomaterials: synthesis, properties, and diverse applications *Nano-Structures & Nano-Objects* **39** 101271
[2] Djurišić A B, Liu X and Leung Y H 2014 Zinc oxide films and nanomaterials for photovoltaic applications *Physica Status Solidi (RRL)—Rapid Research Letters* **8** 123–32
[3] Djurišić A B, Ng A M C and Chen X Y 2010 ZnO nanostructures for optoelectronics: material properties and device applications *Prog. Quantum Electron.* **34** 191–259
[4] Jiang C Y, Sun X W, Lo G Q, Kwong D L and Wang J X 2007 Improved dye-sensitized solar cells with a ZnO-nanoflower photoanode *Appl. Phys. Lett.* **90** 263501
[5] Bagga S, Akhtar J and Mishra S 2018 Synthesis and applications of ZnO nanowire: a review *AIP Conf. Proc.* **1989** 020004
[6] Noman M T, Amor N and Petru M 2022 Synthesis and applications of ZnO nanostructures (ZONSs): a review *Crit. Rev. Solid State Mater. Sci.* **47** 99–141
[7] Mishra Y K and Adelung R 2018 ZnO tetrapod materials for functional applications *Mater. Today* **21** 631–51
[8] Wei J, Yang C, Man B Y, Liu M, Chen C S, Liu A H and Feng L B 2010 Characterization and optical properties of ZnO tetrapod nanorods synthesized by two-step method *Physica* B **405** 1976–9
[9] Guo M Y, Ng A M C, Liu F, Djurišić A B, Chan W K, Su H and Wong K S 2011 Effect of native defects on photocatalytic properties of ZnO *J. Phys. Chem.* C **115** 11095–101
[10] Mishra Y K *et al* 2013 Fabrication of macroscopically flexible and highly porous 3D semiconductor networks from interpenetrating nanostructures by a simple flame transport approach *Part & Part Syst Charact* **30** 775–83
[11] Raha S and Ahmaruzzaman M 2022 ZnO nanostructured materials and their potential applications: progress, challenges and perspectives *Nanoscale Adv.* **4** 1868–925
[12] Siebert L *et al* 2021 Light-controlled growth factors release on tetrapodal ZnO-incorporated 3D-printed hydrogels for developing smart wound scaffold *Adv. Funct. Mater.* **31** 2007555
[13] Nasajpour A *et al* 2021 Nanoengineered antiviral fibrous arrays with rose-thorn-inspired architectures *ACS Materials Lett.* **3** 1566–71
[14] Sui M, Gong P and Gu X 2013 Review on one-dimensional ZnO nanostructures for electron field emitters *Front. Optoelectron.* **6** 386–412
[15] Zhu W 2001 *Vacuum Microelectronics* (Wiley) (https://doi.org/10.1002/0471224332)

[16] Sun L, Ye Z F, Ma L A and Zhang Y A 2022 Improving field emission performance of patterned ZnO electron emission source by optimizing array spacing *Vacuum* **201** 111121
[17] Haugg S, Hedrich C, Zierold R and Blick R H 2022 Field emission characteristics of ZnO nanowires grown by catalyst-assisted MOCVD on free-standing inorganic nanomembranes *J. Phys. D* **55** 255104
[18] Zhang Y A, He L C, Jin T, Guo T L, Zhou X T and Lin Z X 2016 Surface-conducted field emission electron sources with ZnO emitters of different morphologies *J. Alloys Compd.* **688** 77–82
[19] Li Y, Zhang Z, Zhang G, Zhao L, Deng S, Xu N and Chen J 2017 Optimizing the field emission properties of ZnO nanowire arrays by precisely tuning the population density and application in large-area gated field emitter arrays *ACS Appl. Mater. Interfaces* **9** 3911–21
[20] Qian X, Liu H, Guo Y, Song Y and Li Y 2008 Effect of aspect ratio on field emission properties of ZnO nanorod arrays *Nanoscale Res. Lett.* **3** 303
[21] Zhao Y, Chen Y, Zhang G, Zhan R, She J, Deng S and Chen J 2021 High current field emission from large-area indium doped ZnO nanowire field emitter arrays for flat-panel x-ray source application *Nanomaterials* **11** 240
[22] Wu L, Li Q, Zhang X, Zhai T, Bando Y and Golberg D 2011 Enhanced field emission performance of Ga-doped $In_2O_3(ZnO)_3$ superlattice nanobelts *J. Phys. Chem.* C **115** 24564–8
[23] Young S-J, Liu Y-H and Chien J-T 2018 Improving field electron emission properties of ZnO nanosheets with Ag nanoparticles adsorbed by photochemical method *ACS Omega* **3** 8135–40
[24] Kumar P *et al* 2023 Significant enhancement in the cold emission characteristics of chemically synthesized super-hydrophobic zinc oxide rods by nickel doping *Nanoscale Adv.* **5** 6944–57
[25] Zhao Q, Gao J, Zhu R, Cai T, Wang S, Song X, Liao Z, Chen X and Yu D 2010 Ultrahigh field emission current density from nitrogen-implanted ZnO nanowires *Nanotechnology* **21** 095701
[26] Zheng K, Shen H, Li J, Sun D, Chen G, Hou K, Li C and Lei W 2008 The fabrication and properties of field emission display based on ZnO tetrapod-liked nanostructure *Vacuum* **83** 261–4
[27] Zhou X, Lin T, Liu Y, Wu C, Zeng X, Jiang D, Zhang Y and Guo T 2013 Structural, optical, and improved field-emission properties of tetrapod-shaped Sn-doped ZnO nanostructures synthesized via thermal evaporation *ACS Appl. Mater. Interfaces* **5** 10067–73
[28] Al-Tabbakh A A, More M A, Joag D S, Ramgir N S, Mulla I S and Pillai V K 2007 Energy analysis of field emitted electrons from a ZnO tetrapod *Appl. Phys. Lett.* **90** 162102
[29] Jung M N, Ha S H, Oh S J, Koo J E, Cho Y R, Lee H C, Lee S T, Jeon T-I, Makino H and Chang J H 2009 Field emission properties of indium-doped ZnO tetrapods *Curr. Appl Phys.* **9** e169–72
[30] Wan Q, Yu K, Wang T H and Lin C L 2003 Low-field electron emission from tetrapod-like ZnO nanostructures synthesized by rapid evaporation *Appl. Phys. Lett.* **83** 2253–5
[31] Mishra Y K *et al* 2015 Direct growth of freestanding ZnO tetrapod networks for multifunctional applications in photocatalysis, UV photodetection, and gas sensing *ACS Appl. Mater. Interfaces* **7** 14303–16
[32] Fowler R H and Nordheim L 1928 Electron emission in intense electric fields *Proc. R. Soc.* A **119** 173–81
[33] Di Bartolomeo A, Passacantando M, Niu G, Schlykow V, Lupina G, Giubileo F and Schroeder T 2016 Observation of field emission from GeSn nanoparticles epitaxially grown on silicon nanopillar arrays *Nanotechnology* **27** 485707
[34] Kim H, Park C-S and Yu S J 2024 Generalized electron emission theory for one-dimensional conducting *Materials Applied Sciences* **14** 2993
[35] Ang L K, Ang Y S and Lee C H 2023 Universal model for electron thermal-field emission from two-dimensional semimetals *Phys. Plasmas* **30** 033103
[36] Kyritsakis A and Xanthakis J P 2015 Derivation of a generalized fowler–nordheim equation for nanoscopic field-emitters *Proc. R. Soc.* A **471** 20140811
[37] Pakhira N and Mahato R 2023 Role of work function distribution on field emission effects *Physica B* **670** 415394
[38] Jensen K L 2019 A reformulated general thermal-field emission equation *J. Appl. Phys.* **126** 065302
[39] Giubileo F, Iemmo L, Passacantando M, Urban F, Luongo G, Sun L, Amato G, Enrico E and Di Bartolomeo A 2019 Effect of electron irradiation on the transport and field emission properties of few-layer MoS_2 field-effect transistors *J. Phys. Chem.* C **123** 1454–61
[40] Giubileo F, Passacantando M, Urban F, Grillo A, Iemmo L, Pelella A, Goosney C, LaPierre R and Di Bartolomeo A 2020 Field emission characteristics of InSb patterned nanowires *Adv. Electron. Mater.* **6** 2000402
[41] Bhattacharya R, Turchetti M, Keathley P D, Berggren K K and Browning J 2021 Long term field emission current stability characterization of planar field emitter devices *Journal of Vacuum Science & Technology* B **39** 053201